ACS APPLIED MATERIALS & INTERFACES

Research Article

www.acsami.org

Micromechanism in Self-Lubrication of TiB_2/Al Composite

Xin Zhou,[†,§] Longtao Jiang,[‡] Shengbin Lei,*[,§] Wei Quan Tian,*[,†] and Gaohui Wu*[,‡]

[†]State Key Laboratory of Urban Water Resource and Environment, Institute of Theoretical and Simulational Chemistry, Academy of Fundamental and Interdisciplinary Sciences, Harbin Institute of Technology, Harbin, 150080, P. R. China

[‡]Institute of Metal Matrix Composite Science and Engineering, Harbin Institute of Technology, Harbin, 150080, P. R. China

[§]State Key Laboratory of Robotics and System, Harbin Institute of Technology, Harbin, 150080, P. R. China

Supporting Information

ABSTRACT: The authors discovered the self-lubrication behavior of TiB_2/Al composite and pointed out that the materials responsible for the self-lubrication behavior comes from the oxidation of TiB_2. Atomic/friction force microscopy and first-principles calculations have been employed to study the self-lubrication microscopic mechanism of TiB_2/Al composite. Atomic force microscopy confirms the existence of a soft film with nanometer thickness on the TiB_2 surface, which was attributed to H_3BO_3 film. Friction measurements revealed much smaller friction force on this H_3BO_3 nanofilm than that on Al matrix. The detailed structure and interactions among H_3BO_3 molecules and between the H_3BO_3 sheet and substrate were explored by density functional theory based calculations. The details of adsorption of H_3BO_3 sheet on TiB_2 and TiO_2 surface were scrutinized and the potential of the relative movement between H_3BO_3 sheets were scanned and compared with that of graphite. The generation of H_3BO_3 film, the strong chemical adsorption of H_3BO_3 film on the surface of the composite, the strong hydrogen bonding in H_3BO_3 film, and small potential in the relative slide between H_3BO_3 sheets warrant the good self-lubricant properties of TiB_2/Al metal matrix composites.

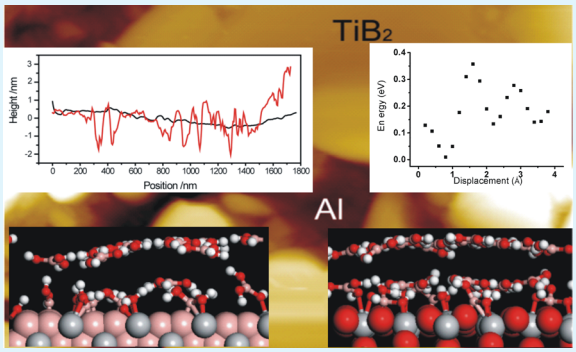

KEYWORDS: *TiB_2/Al composite, self-lubrication microscopic mechanism, friction measurements, H_3BO_3 sheets, hydrogen bond, first-principles calculations*

INTRODUCTION

TiB_2/Al, low cost metal matrix composites (MMC), have significant strain rate sensitivity at high strain rates, and exhibit high flow stress[1] and good wear resistance.[2−4] The TiB_2/Al MMC has strong interfacial bonding between Al matrix and TiB_2 particles, thus showing high stability.[5−7] So far, most TiB_2/Al MMCs were fabricated using in situ method.[8−13] However, during the process of in situ fabrication, due to the difficulty in controlling particle size and reaction speed as well as generation of some brittle compounds at the interface (such as Al_3Ti), the properties of the TiB_2/Al composite could be significantly affected.[14] To avoid the negative effect, TiB_2/Al MMC was fabricated by squeeze casting technology (SCT).[15,16] TiB_2/Al MMC fabricated with SCT exhibits high wear resistance and no obvious adhesion or abrasion wear was observed on worn surfaces of TiB_2/Al composites.[16] Most importantly, friction coefficient of TiB_2/Al MMC is very low in a wide range of volume ratio of TiB_2 and Al.[16,17] The low friction coefficient was ascribed to the formation of H_3BO_3 on the surface of MMC due to the generation of B_2O_3 from TiB_2.[4,16−19]

Until now, few works have been carried out in the field of micro tribology of boric acid, although investigations on the macro tribological behaviors of boric acid have been reported.[20] Atomic force microscopy(AFM) based studies[21] found that under nanoscale contact, the boric acid film with deformed surface after the sliding of AFM tips shows low friction. This was ascribed to the reorientation of the boric acid sheets upon the deformation by the AFM tip.[22] However, the micromechanism for the lubrication of TiB_2/Al MMC including the interface structure between TiB_2/Al and H_3BO_3 and the lubrication mechanism of H_3BO_3 on the MMC surface is not yet clear. Such micromechanism studies may help to optimize the design of new self-lubricant composite materials.

In the present work, the microstructure of TiB_2/2024Al MMC and the mechanism of self-lubrication of the materials are investigated with atomic/friction force microscopy (AFM/FFM) and first-principles based calculations. During the wear process of TiB_2/2024Al MMC, the Al matrix supports the TiB_2 particles and wears away from the surface of the composites due to its relatively lower hardness. The TiB_2 left on the MMC surface is oxidized to TiO_2 and B_2O_3 followed by the formation of H_3BO_3 with H_2O on the surface of the composites.[5,16] Two different interfaces could form after the formation of H_3BO_3.

Received: January 22, 2015
Accepted: May 26, 2015
Published: May 26, 2015

ACS Publications © 2015 American Chemical Society

DOI: 10.1021/acsami.5b02906
ACS Appl. Mater. Interfaces 2015, 7, 12688−12694

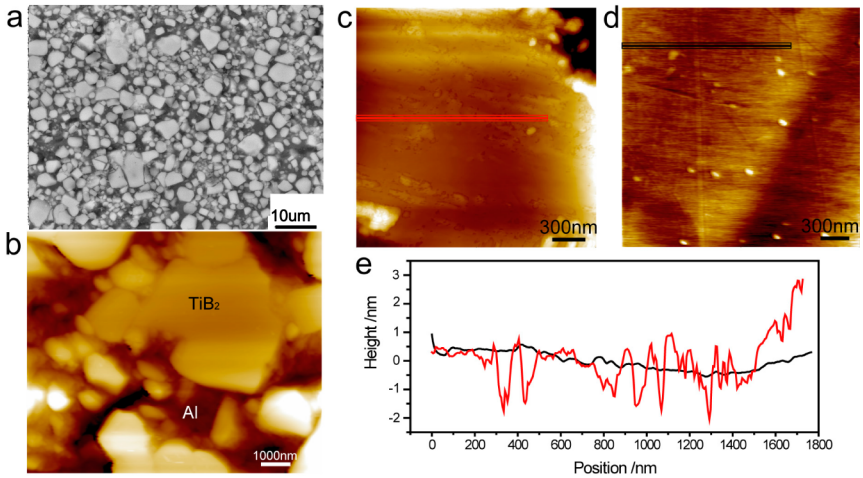

Figure 1. (a) Large-scale SEM image of TiB_2/2024Al MMC. (b) Large-scale AFM height image (contact mode) of the polished TiB_2/2024Al MMC surface. TiB_2 particles are distributed in the Al matrix homogeneously. Panels c and d are the height images obtain on the TiB_2 particle surface with tapping and contact mode, respectively. Cross section profile (e) clearly shows the difference in surface roughness.

One is H_3BO_3/TiB_2 and the other one is H_3BO_3/TiO_2. Whether H_3BO_3 could adsorb on the surface is crucial to the self-lubrication of the material. In this work we first confirm the existence of a soft lubricate layer on the TiB_2 particle surface by AFM characterization, and the lateral friction measurements indicate the friction force is reduced for about 24.5 times on the TiB_2 particle surface in comparison with that on Al matrix. Then the structure of H_3BO_3 adsorbed surfaces is studied with first-principles calculations and the microscopic mechanism of the self-lubrication is revealed in detail.

■ EXPERIMENTAL AND COMPUTATIONAL DETAILS

Sample Preparation and Characterization. The TiB_2/2024Al MMC (55 vol % of TiB_2) was prepared by pressure infiltration method. The average size of TiB_2 is 1.6 μm. The preheating temperature of preform is between 600−610 °C with the heating rate of 10 °C/s under the atmospheric environment and retained at the high temperature stage for 1h. At 770 °C, the molten 2024Al is extruded into the preform under a pressure of 70 MPa. Figure 1a shows the microscopic SEM image of TiB_2/2024Al MMC, from which it can be seen that the TiB_2 particles are evenly distributed. The composition of the samples were analyzed by transmission electron microscope (TEM) and X-ray photoelectron spectroscopy (XPS), which were conducted on a JEOL200CX transmission electron microscope and PHI5700 ESCA system X-ray photoelectron spectroscopy, respectively. Both TEM and XPS characterizations confirmed the oxidation of TiB_2 and formation of TiO_2 and B_2O_3 on the sample surface (Supporting Information Figures S1 and S2).[19]

AFM/FFM measurements were performed with an Agilent 5100 Scanning Probe Microscopy, operating with tapping mode and friction mode. The AFM probe used for tapping mode measurements is Tap300Al-G from Budget sensors, a silicon AFM probe coated with aluminum, and the resonant frequency is 300 kHz. For friction measurements a ContAl-G probe with aluminum reflection coating (resonant frequency = 13 kHz, force constant = 0.2 N/m) was used.

Models and Computational Details. Small H_3BO_3 clusters up to 13 H_3BO_3 molecules are constructed to study the strength of hydrogen bonds in the H_3BO_3 sheet. Density functional theory based first-principles methods B3LYP[23,24] with 6-31G(d, p)[25,26] basis were employed for this characterization. The Gaussian 03 program[27] was used for those calculations. Two models, H_3BO_3/TiB_2 and H_3BO_3/TiO_2, are designed for the interface between H_3BO_3 and the TiB_2/Al MMC. The (110) surface is chosen as the model for both TiB_2 and TiO_2.

The surface adsorption simulations are performed with VASP package with projector augmented wave (PAW) pesudopotentials.[28,29] The exchange-correlation functional utilized was at the generalized gradient approximation level, known as GGA-PBE.[30] A plane-wave basis set with a cutoff energy of 400 eV was used for electron wave function. A Monkhost−Pack mesh of 3 × 3 × 1 k-points was used for sampling the Brillouin zone during ionic relaxation, which is large enough for the current simulation. Optimization of structures was converged until the force on each atom is less than 1×10^{-2} eV.nm^{-1}, and energies were converged to 1×10^{-5} eV. In this work, 19.37 Å × 20.96 Å × 23.03 Å is chosen for the supercell of TiB_2 cell and 20.71 Å × 25.99 Å × 23.25 Å is chosen for that of TiO_2, the large vacuum space used in the supercells can avoid the interaction between the surface cells and their images along the *z*-axes. Three layers of TiO_2 and TiB_2 containing 210 and 216 atoms are used to mimic the surface of TiO_2(110) and TiB_2(110), respectively, while H_3BO_3 cluster adsorbed onto surface is composed of 12 H_3BO_3 molecules.

■ RESULTS AND DISCUSSION

Microstructure and Friction Measurements. Scanning probe microscopy (including STM, AFM, FFM, etc.) provides very powerful tool for the characterization of surface structures and physical/chemical properties on the nanoscale.[31−33] In this work AFM, both tapping and contact mode, in combination with FFM was used to characterize the surface structure and probe the mechanism of lubrication. Large scale SEM and AFM height image reveals that the TiB_2 particles are distributed homogeneously in the Al matrix. The TiB_2 particles exhibit larger height in comparison with the Al matrix, and the top surface is flat because of polishing. Scratches are observed on the particle surface, appearing as depressions in height image obtained with contact mode. However, on the height image obtained with tapping mode, no scratches appear, instead, the surface is covered by a film with nanometer thickness (Figure 1). The roughness measured from the tapping mode image is apparently larger than that obtained from contact mode as shown in the section profile of both images (Figure 1d). These evidence indicate that there exists a soft film on the particle surface, which can be removed by tip scratching when operated with contact mode. This hypothesis is also supported by the phase image (Supporting Information Figure S3), which reveals quite different contrast on the TiB_2 particle surface in comparison with the Al matrix. This soft film is attributed to H_3BO_3, which was formed during the preheating and friction

DOI: 10.1021/acsami.5b02906
ACS Appl. Mater. Interfaces 2015, 7, 12688−12694

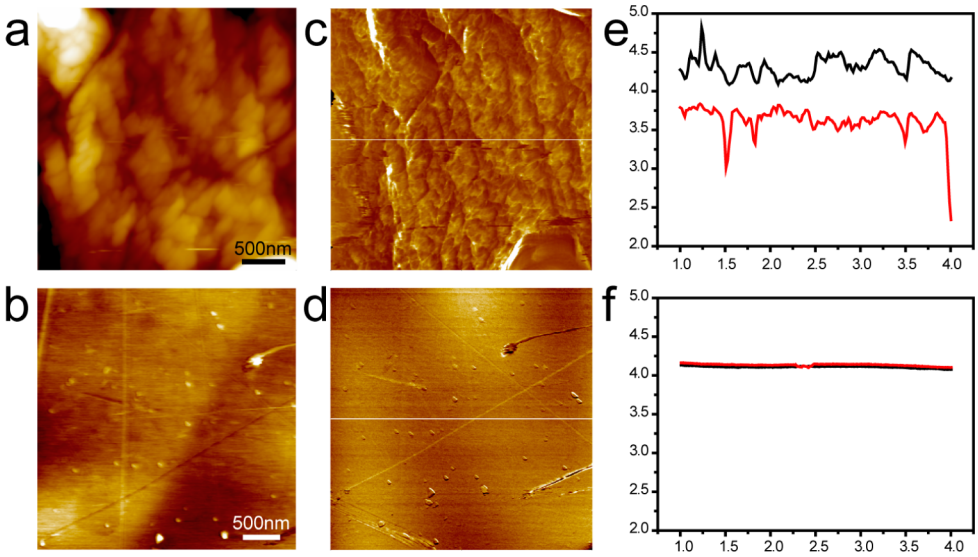

Figure 2. Height (a and b) and friction image (c and d) obtained on the Al matrix and TiB_2 particle surface. The cross section profiles of the trace and retrace channel (e and f) show clearly the difference in lateral friction forces on these different materials.

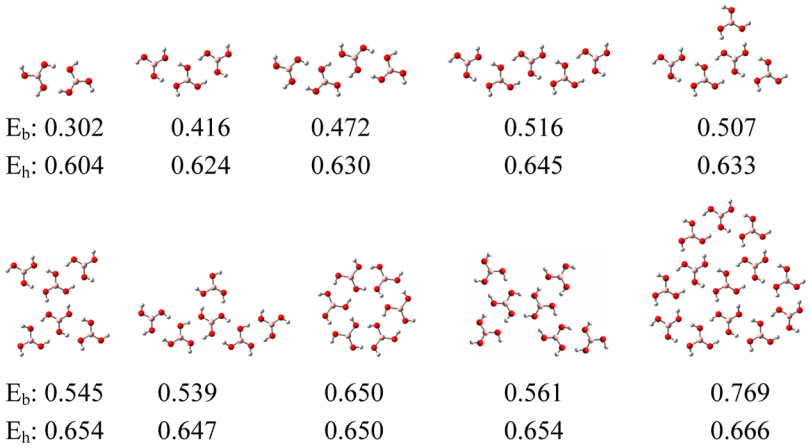

Figure 3. H_3BO_3 cluster sheets with hydrogen bonds. E_b is binding energy per H_3BO_3 (in eV), and E_h is hydrogen bond energy per H-bond pair (in eV).

process. The oxidation was confirmed by the TEM and XPS analysis (Supporting Information Figure S1 and S2).

The lateral friction forces on both TiB_2 and Al matrix using friction force microscopy are shown in Figure 2. Friction measurement on the TiB_2 particle surface and Al matrix, respectively, with the same tip and operation parameters, were performed, and cross section profile from the trace and retrace of friction channel were obtained (Figure 2). The gap between the trace and retrace profile allows to compare the friction forces qualitatively. The friction force in the same image was not measured and compared for the two components due to the big difference in height of both components, and the surface morphology can strongly convolute into the friction force. The friction force on the TiB_2 particle surface is reduced about 24.5 times with respect to that on Al matrix. The AFM measurements confirmed the existence of a soft film of H_3BO_3 with nanometer thickness.[34] The reduction of friction forces is attributed to the lubrication properties of the H_3BO_3 film on the TiB_2 particle surface.

First-Principles Calculations. The structure of H_3BO_3 cluster sheets and strength of interaction among H_3BO_3 molecules in the H_3BO_3 cluster sheets are investigated first. H_3BO_3 has C_3 symmetry and a H_3BO_3 molecule can form three pairs of hydrogen bonds with its surrouding H_3BO_3 molecules. The OH bond distance is 0.96 Å in a H_3BO_3 and it lengthens to about 0.98 Å upon forming hydrogen bond with other H_3BO_3. Figure 3 shows the interactions among H_3BO_3 molecules in H_3BO_3 cluster sheet from two to 13 H_3BO_3 molecules. As shown in Figure 3, binding energy (E_b) and hydrogen bond energy (E_h) are calculated to estimate the strength of H_3BO_3 nanosheet. E_b is the binding energy per H_3BO_3 molecule ($E_b = E_{tot}/n$, E_{tot} is the total binding energy of the system, and n is the number of H_3BO_3), and E_h is hydrogen bond energy per pair of hydrogen bonds ($E_h = E_{tot}/n_{pair}$, n_{pair} is the number of hydrogen bond pairs, for example, a H_3BO_3 dimer has one hydrogen bond pair). As the size of H_3BO_3 nanosheet increases, $E_h = 2E_b/3$. As can be seen from E_b valuess and E_h values in Figure 3, E_h does not change much with the size of H_3BO_3 sheet and E_h may converge to a value around 0.700 eV, and following this estimation E_b could reach about 1.000 eV. The strong hydrogen bonding in H_3BO_3 mesh ensure the stress and strain resistance of the film.

The adsorption of single H_3BO_3 layer (with 12 H_3BO_3 molecules) on the (110) TiB_2 surface is shown in Figure 4a.

DOI: 10.1021/acsami.5b02906
ACS Appl. Mater. Interfaces 2015, 7, 12688−12694

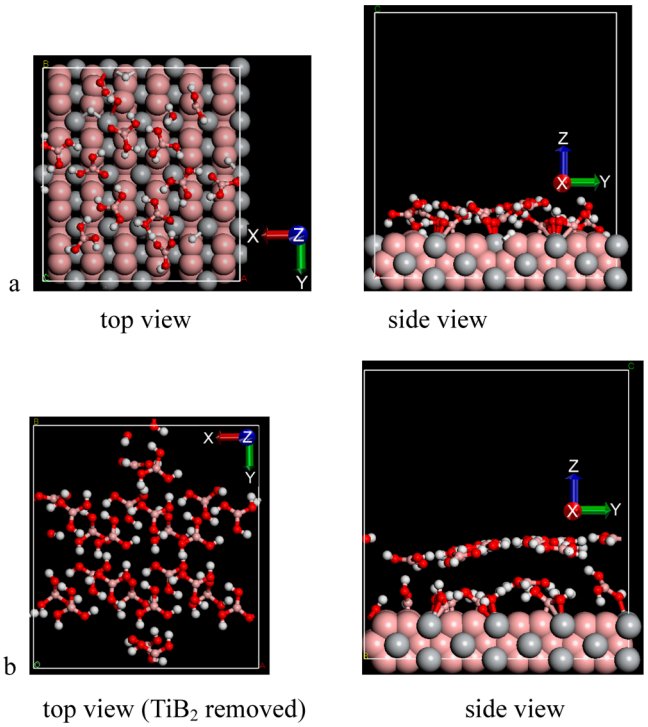

Figure 4. Adsorption of single layer (a) and double layer (b) H_3BO_3 on (110) TiB_2 surface.

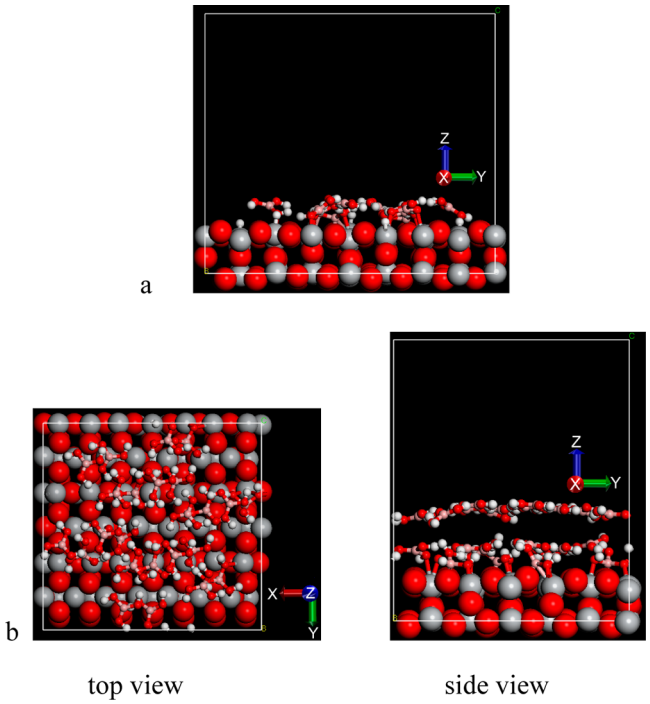

Figure 5. Adsorption of single layer (a) and double layer (b) H_3BO_3 on (110) TiO_2 surface.

The mesh shape of the H_3BO_3 sheet on TiB_2 surface remains and conspicous deformation of the H_3BO_3 sheet occurs. Such deformation comes from the chemical bonding between the H_3BO_3 sheet and the TiB_2 surface. The $B(TiB_2)-B(H_3BO_3)$ distance ranges from 1.85 to 3.10 Å and the $Ti(TiB_2)-B(H_3BO_3)$ distance ranges from 2.20 to 2.80 Å. The binding energy between the H_3BO_3 sheet and the TiB_2 surface is −53.100 eV, that is, −4.425 eV per H_3BO_3 molecule. This strong adsorption warranties the good wear properties of H_3BO_3 during sliding of the intersurfaces.

The adsorption of double layers of H_3BO_3 on the (110) TiB_2 surface is shown in Figure 4b. The upper layer H_3BO_3 does not affect the adsorption of the lower layer H_3BO_3 on TiB_2. The average distance between those two H_3BO_3 layers is 3.66 Å and the average distance between the lower layer H_3BO_3 and TiB_2 is 2.55 Å. The average hydrogen bond distance in both layers of H_3BO_3 is 1.68 Å. The interaction energy between the upper layer and the rest of the system is −0.69 eV. Such weak attraction and van der Waals type distance (3.66 Å) ensure the smooth sliding of the upper layer H_3BO_3 with respect the surface.

Figure 5a shows the adsorption of single H_3BO_3 layer (with 12 H_3BO_3 molecules) on (110) TiO_2 surface, and conspicuous doformation of the H_3BO_3 sheet from plane occurs. The distance from $B(H_3BO_3)$ to $O(TiO_2)$ ranges from 1.49 to 3.32 Å and the distance from $Ti(TiO_2)$ to $B(H_3BO_3)$ ranges from 2.59 to 3.50 Å. The average distance from H_3BO_3 sheet to TiO2 surface is 2.05 Å. Such strong deformation comes from the strong chemical adsorption of H_3BO_3 on TiO_2 surface, and possibly the limited size of the model which cause some edge effect, that is, the edge of H_3BO_3 sheet has strong interaction with the TiO_2 surface. Both effects reveal the strong interaction of H_3BO_3 with TiO_2. The adsorption energy of this H_3BO_3 layer onTiO_2 is −70.4 eV, which obviously manifest the nature of strong chemical adsorption. Eventhough, the strong hydrogen bonds (with average hydrogen bond distance of 1.91 Å) in the H_3BO_3 sheet tightly bind the H_3BO_3 molecules.

The adsorption of the second layer H_3BO_3 on H_3BO_3/TiO_2 elongates the average distance between the singly adsorbed H_3BO_3 layer and TiO_2 from 2.05 to 2.76 Å. However, the strong bonding nature of the first (lower) H_3BO_3 layer with TiO_2 remains as shown in Figure 5b, and the network of the lower H_3BO_3 layer is enhanced by the adsorption of the upper H_3BO_3 layer with average hydrogen bond distance of 1.76 Å. The average hydrogen bond distance of the upper H_3BO_3 layer is 1.75 Å. The distance between the two H_3BO_3 layers is 3.41 Å, slightly shorter than that when adsorbed on TiB_2 (3.66 Å). The adsorption enenrgy of the upper H_3BO_3 layer is −0.49 eV and this weak attraction facilitates the sliding among H_3BO_3 layers.

The potential energy during the relative sliding of two H_3BO_3 sheets is investigated as shown in Figure 6. The equilibrium distance between two H_3BO_3 sheets is located to be 3.70 Å. The stress imposed on the H_3BO_3 sheet during sliding will push the two H_3BO_3 sheets closer than the equilibrium distance. For the simulation of relative sliding of H_3BO_3 sheets, the distance between the two H_3BO_3 sheets is 3.05 Å. The energy barrier from the energy minimum to energy maximum of sliding in one direction (oa) is 0.14 eV. The other direction needs higher energy (0.37 eV) to overcome the potential energy barrier.

Graphite is a well-know solid lubricant. The potential energy is investigated in the present work for comparison with that of H_3BO_3 layers. The equilibrium distance between two grapheme sheets is 4.25 Å at the same level of theory. To simulate the raltive sliding of two graphene sheets under some stress, the distance between two graphene sheets is taken as 3.40 Å. The potential energy of relative sliding along one direction (oa) is 0.34 eV and it is about 0.82 eV along the other direction as shown in Figure 7. Both potential energies are larger than the corresponding values of H_3BO_3 sheets. A conservative

DOI: 10.1021/acsami.5b02906
ACS Appl. Mater. Interfaces 2015, 7, 12688−12694

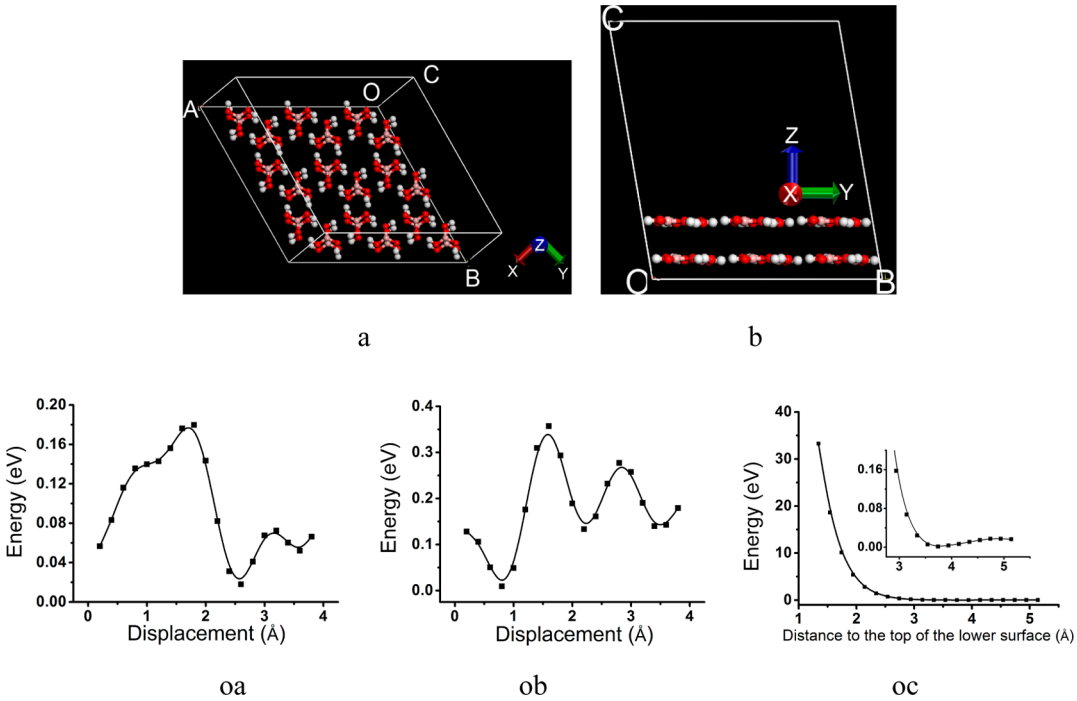

Figure 6. Potential energy of relative movement between two H_3BO_3 layers. oa, ob, and oc are the three directions as shown in a and b.

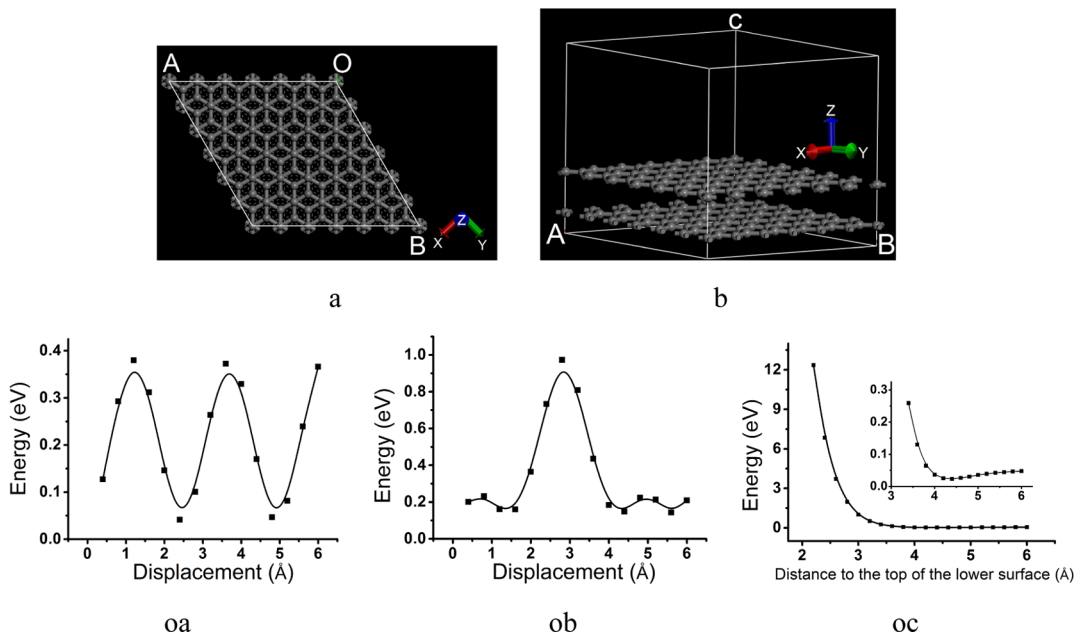

Figure 7. Potential energy of relative movement between two graphene layers. oa, ob, and oc are the three directions as shown in a and b.

observation about the relative sliding of H_3BO_3 sheets is that the friction of H_3BO_3 sheet is comparable to that of graphite (or graphene sheets), that is, H_3BO_3 nanosheets have good lubrication.

In summary, the oxidization of TiB_2 on the surface of TiB_2/Al MMC forming H_3BO_3 leads to the formation of graphite like network of H_3BO_3. The strong hydrogen bonds in the H_3BO_3 sheet make this network strong enough to be wear resistant, while the small potential energy along the relative movement between H_3BO_3 sheets warrants the good lubrication of the H_3BO_3 film on the TiB_2/Al surface. Self-supply of H_3BO_3 through tribo-chemical reactions ensure the self-lubrication cycle.

CONCLUSION

The microstructure and lubrication mechanism of TiB_2/2024Al MMC surface have been studied with both AFM/FFM and first-principles calculations. AFM characterizations confirmed the existence of a soft nanometer film on the surface of TiB_2 particles, and FFM reveals significant reduction of lateral friction forces on the TiB_2 surface (24.5 times smaller in comparison with Al matrix). The strength of H_3BO_3 network and adsorption of H_3BO_3 sheets on the surfaces of TiO_2 and

DOI: 10.1021/acsami.5b02906
ACS Appl. Mater. Interfaces 2015, 7, 12688−12694

TiB_2 have been investigated in detail with first-principles calculations. H_3BO_3 can be stably adsorbed on TiB_2 and TiO_2 surfaces through chemical bond between the first layer of H_3BO_3 film and those surfaces, ensuring the stability of the film. The strong hydrogen bonds among H_3BO_3 render the formation of graphene like network, and this warrants the wear resistance of H_3BO_3. The relative weak interaction between H_3BO_3 layers is responsible for the good self-lubricant properties of this material on TiB_2 or TiO_2.

■ ASSOCIATED CONTENT

Ⓢ Supporting Information

Height and phase image and TEM and XPS of the TiB_2/Al composite. The Supporting Information is available free of charge on the ACS Publications website at DOI: 10.1021/acsami.5b02906.

■ AUTHOR INFORMATION

Corresponding Authors

*E-mail: leisb@hit.edu.cn
*E-mail: tianwq@hit.edu.cn.
*E-mail: wugh@hit.edu.cn.

Notes

The authors declare no competing financial interest.

■ ACKNOWLEDGMENTS

The work is supported by National Key Laboratory of Materials Behaviors & Evaluation Technology in Space Environments(HIT), the National Science Foundation of China (21303030, 21173061, 21373070), the State Key Lab of Urban Water Resource and Environment (HIT) (2014TS01) and the Open Project of State Key laboratory of Supramolecular Structure and Materials (JLU) (SKLSSM2015018), the Open Project of State Key Laboratory of Robotics and System (HIT) (SKLRS-2015-MS-11).

■ REFERENCES

(1) Zhu, D. Z.; Wu, G. H.; Chen, G. Q.; Zhang, Q. Dynamic Deformation Behavior of a High Reinforcement Content TiB_2/Al Composite at High Strain Rates. *Mater. Sci. Eng., A* **2008**, *487*, 536−540.

(2) Natarajan, S.; Narayanasamy, R.; Kumaresh Babu, S. P.; Dinesh, G.; Anil Kumar, B.; Sivaprasad, K. Sliding Wear Behaviour of Al 6063/TiB_2 in situ Composites at Elevated Temperatures. *Mater. Design* **2009**, *30*, 2521−2531.

(3) Smith, A. V.; Chung, D. D. L. Titanium Diboride Particle-Reinforced Aluminium with High Wear Resistance. *J. Mater. Sci.* **1996**, *31*, 5961−5973.

(4) Sreenivasan, A.; Vizhian, S. P.; Shivakumar, N. D.; Muniraju, M.; Raguraman, M. A Study of Microstructure and Wear Behaviour of TiB_2/Al Metal Matrix Composites. *Lat. Am. J. Solids Struct.* **2011**, *8*, 1−8.

(5) Caracostas, C. A.; Chiou, W. A.; Fine, M. E.; Cheng, H. S. Tribological Properties of Aluminum Alloy Matrix TiB_2 Composite Prepared by In-Situ Processing. *Metall. Mater. Trans. A* **1997**, *28A*, 491−502.

(6) Suresh, S.; Moorthi, N.; Shenbaga, V.; Selvakumar, N.; Vettivel, S. C. Tribological, Tensile and Hardness Behavior of TiB_2 Reinforced Aluminum Metal Matrix Composite. *J. Balk. Tribol. Assoc.* **2014**, *20*, 380−394.

(7) Mitra, R.; Chiou, W. A.; Fine, M. E.; Weertman, J. R. Interfaces in as-extruded XD Al/TiC and Al/TiB_2 Metal Matrix Composites. *J. Mater. Res.* **1993**, *8*, 2380−2392.

(8) Sadeghian, Z.; Enayati, M. H.; Beiss, P. In-Situ Production of Al-TiB_2 Nanocomposite by Double-Step Mechanical Alloying. *J. Mater. Sci.* **2009**, *44*, 2566−2572.

(9) Katakam, S.; Asiamah, N.; Santhanakrishnan, S.; Dahotre, N. Laser In-Situ Synthesis of TiB_2−Al Composite Coating for Improved Wear Performance. *Surf. Coat. Technol.* **2013**, *236*, 200−206.

(10) Gotman, I.; Koczak, M. J.; Shtessel, E. Fabrication of Al Matrix In-situ Composites via Self-Propagating Synthesis. *Mater. Sci. Eng. A* **1994**, *187*, 189−199.

(11) Brinkman, H. J.; Duszczyk, J.; Katgerman, L. In-Situ Formation of TiB_2 in a Aluminum Matrix. *Scr. Mater.* **1997**, *37*, 293−297.

(12) Feng, C. F.; Froyen, L. Microstructures of In Situ Al/TiB_2 MMCs Prepared by a Casting Route. *J. Mater. Sci.* **2000**, *35*, 837−850.

(13) Tayeh, T.; Douin, J.; Jouannigot, S.; Zakhour, M.; Nakhl, M.; Silvain, J.; Bobet, J. Hardness and Young's Modulus Behavior of Al Composites Reinforced by Nanometric TiB_2 Elaborated by Mechanosynthesis. *Mater. Sci. Eng. A* **2014**, *591*, 1−8.

(14) Tee, K. L.; Lu, L.; Lai, M. O. Improvement in Mechanical Properties of In-Situ Al−Ti_{B2} Composite by Incorporation of Carbon. *Mater. Sci. Eng. A* **2003**, *339*, 227−231.

(15) Zhao, M.; Wu, G. H.; Dou, Z. Y.; Jiang, L. T. TiB_{2p}/Al Composite Fabricated by Squeeze Casting Technology. *Mater. Sci. Eng. A* **2004**, *374*, 303−306.

(16) Zhao, M.; Wu, G. H.; Jiang, L. T.; Dou, Z. Y. Friction and Wear Properties of TiB_{2p}/Al Composite. *Compos. Part A* **2006**, *37*, 1916−1921.

(17) Zhao, M.; Wu, G. H.; Dou, Z. Y.; Jiang, L. T. Property Characteristics of a TiB_{2P}/Al Composite Fabricated by Squeeze Casting Technology. *J. Mater. Sci. Technol.* **2006**, *22*, 83−86.

(18) Dvorak, D.; Wahl, K. J.; Singer, I. L. Friction Behavior of Boric Acid and Annealed Boron Carbide Coatings Studied by In Situ Raman Tribometry. *Tribol. Trans.* **2002**, *45*, 354−362.

(19) Tian, S. F.; Jiang, L. T.; Guo, Q.; Wu, G. H. Effect of Surface Roughness on Tribological Properties of TiB_2/Al Composites. *Mater. Design* **2014**, *53*, 129−136.

(20) Erdemir, A. Tribological Properties of Boric-Acid and Boric-Acid-Forming Surfaces 0.1. Crystal-Chemistry and Mechanism of Self-Lubrication of Boric-Acid. *Lubr. Eng.* **1991**, *47*, 168−173.

(21) Ma, X. D. Nanotribological Properties of Boric Acid−Boron Oxide system. *Mater. Mech. Eng.* **2000**, *24*, 11−19.

(22) Ma, X. D. Nanoscale Tribological Properties of Boric Acid. *Lubr. Eng.* **1999**, *3*, 29−39.

(23) Becke, A. D. Density−Functional Thermochemistry. III. The Role of Exact Exchange. *J. Chem. Phys.* **1993**, *98*, 5648−5652.

(24) Lee, C.; Yang, W.; Parr, R. G. Development of the Colle−Salvetti Correlation-Energy Formula into a Functional of the Electron Density. *Phys. Rev. B* **1988**, *37*, 785−789.

(25) Petersson, G. A.; Bennett, A.; Tensfeldt, T. G.; AI-Laham, M. A.; Shirley, W. A.; Mantzaris, J. A Complete Basis Set Model Chemistry. I. The Total Energies of Closed-Shell Atoms and Hydrides of the First-Row Elements. *J. Chem. Phys.* **1998**, *89*, 2193−2218.

(26) Hariharan, P. C.; Pople, J. A. The Influence of Polarization Functions on Molecular Orbital Hydrogenation Energies. *Theor. Chim. Acta* **1973**, *28*, 213−222.

(27) Frisch, M. J.; Trucks, G. W.; Schlegel, H. B.; Scuseria, G. E.; Robb, M. A.; Cheeseman, J. R.; Montgomery, J. A., Jr.; Vreven, T.; Kudin, K. N.; Burant, J. C.; Millam, J. M.; Iyengar, S. S.; Tomasi, J.; Barone, V.; Mennucci, B.; Cossi, M.; Scalmani, G.; Rega, N.; Petersson, G. A.; Nakatsuji, H.; Hada, M.; Ehara, M.; Toyota, K.; Fukuda, R.; Hasegawa, J.; Ishida, M.; Nakajima, T.; Honda, Y.; Kitao, O.; Nakai, H.; Klene, M.; Li, X.; Knox, J. E.; Hratchian, H. P.; Cross, J. B.; Bakken, V.; Adamo, C.; Jaramillo, J.; Gomperts, R.; Stratmann, R. E.; Yazyev, O.; Austin, A. J.; Cammi, R.; Pomelli, C.; Ochterski, J. W.; Ayala, P. Y.; Morokuma, K.; Voth, G. A.; Salvador, P.; Dannenberg, J. J.; Zakrzewski, V. G.; Dapprich, S.; Daniels, A. D.; Strain, M. C.; Farkas, O.; Malick, D. K.; Rabuck, A. D.; Raghavachari, K.; Foresman, J. B.; Ortiz, J. V.; Cui, Q.; Baboul, A. G.; Clifford, S.; Cioslowski, J.; Stefanov, B. B.; Liu, G.; Liashenko, A.; Piskorz, P.; Komaromi, I.; Martin, R. L.; Fox, D. J.; Keith, T.; Al-Laham, M. A.; Peng, C. Y.;

DOI: 10.1021/acsami.5b02906
ACS Appl. Mater. Interfaces 2015, 7, 12688−12694

Nanayakkara, A.; Challacombe, M.; Gill, P. M. W.; Johnson, B.; Chen, W.; Wong, M. W.; Gonzalez, C.; Pople, J. A. *Gaussian 03*, revision B.03; Gaussian, Inc.: Wallingford, CT, 2004.
(28) Blöchl, P. E. Projector Augmented-Wave Method. *Phys. Rev. B* **1994**, *50*, 17953−17979.
(29) Kresse, G.; Joubert, J. From Ultrasoft Pseudopotentials to the Projector Augmented Wave Method. *Phys. Rev. B* **1999**, *59*, 1758−1775.
(30) Perdew, J. P.; Burke, K.; Ernzerhof, M. Generalized Gradient Approximation Made Simple. *Phys. Rev. Lett.* **1996**, *77*, 3865−3868.
(31) Barth, C.; Foster, A. S.; Henry, C. R.; Shluger, A. L. Recent Trends in Surface Characterization and Chemistry with High-resolution Scanning Force Methods. *Adv. Mater.* **2011**, *23*, 477−501.
(32) Liscio, A.; Palermo, V.; Samorì, P. Nanoscale Quantitative Measurement of the Potential of Charged Nanostructures by Electrostatic and Kelvin Probe Force Microscopy: Unraveling Electronic Processes in Complex Materials. *Acc. Chem. Res.* **2010**, *43*, 541−550.
(33) Riet, J.; Smit, T.; Gerritsen, J. W.; Cambi, A.; Elemans, J. A. A. W.; Figdor, C. G.; Speller, S. Molecular Friction as a Tool to Identify Functionalized Alkanethiols. *Langmuir* **2010**, *26*, 6357−6366.
(34) Erdemir, A.; Fenske, G. R.; Erck, R. A. A Study of the Formation and Self-lubrication Mechanisms of Boric Acid Films on Boric Oxide Coatings. *Surf. Coat. Technol.* **1990**, *43*−*44*, 588−596.

DOI: 10.1021/acsami.5b02906
ACS Appl. Mater. Interfaces 2015, 7, 12688−12694